Heliyon 6 (2020) e03622

Contents lists available at ScienceDirect

Heliyon

journal homepage: www.cell.com/heliyon

Research article

Thermo-elastic behaviour of carbon-fiber reinforced polymer and the effect of adding nanoparticles at elevated heat intensity

Chukwugoize Jekwu Ejeh [a,*], Imad Barsoum [a], Goodnews Ogbegbe Chizindu [b], Graham Martey Kodie [b], Josiah Ikechukwu Anachuna [b]

[a] Mechanical Engineering Department, Khalifa University, Abu Dhabi, United Arab Emirates, P.O Box: 127788, Abu Dhabi, United Arab Emirates
[b] Oil and Gas Engineering Department, All Nations University College, Koforidua, Ghana, P.O Box: 1908, Koforidua, Ghana

ARTICLE INFO

Keywords:
Materials science
Structural engineering
Computational materials science
Materials application
Materials mechanics
Materials structure
Carbon fiber reinforced polymer
Composite materials
Thermo-elastic deformation
Deposited heat power
Thermal-structural analysis

ABSTRACT

Thermal stress development in materials could lead to structural failure in engineering applications. Carbon-fiber reinforced polymer composite (CFRP) have gained wide acceptance in the manufacturing industry. However, its thermo-elastic behaviour at elevated temperatures still remains an open question. Heat transfer analysis coupled with material layer-wise arrangement technique of the CFRP was implemented to investigate the thermo-elastic behaviour of these composites. A finite element model (FEM) was built and studied using COMSOL Multiphysics software. The heat energy applied in the simulation was sourced from a heat beam model. The deposited beam power was varied from 10 to 200W, and focused at the centre of the laminate (y_p = 0.15 m). The laminates considered were made up of six layers with distinctly different stacking sequences. The thermal stresses and strains obtained from the finite element analysis were assessed to observe the material's behaviour when subjected to increasing thermal load. Results revealed that thermal stresses are intense along fiber-direction of the composite laminates. The CFRP material was found to give good thermo-elastic characteristics at lower deposited heat power, however, this was not the case for higher deposited heat power (e.g. 200 W). The anisotropic property of the laminate had a significant influence in managing the thermal stresses. The study was repeated for carbon fibers doped with nanoparticles of silicon carbide (CFSiC) and resin bonded glass fiber (RBGF). It was found that the results were distinctly different when compared with the CFRP laminate. CFSiC showed to exhibit an enhanced thermo-elastic behaviour, due to the high thermal stability of SiC nanoparticles in the composite.

1. Introduction

To achieve the combined advantage of chemical, mechanical and thermal properties in engineering materials, the use of different materials is necessary [1, 2, 3]. The outcome of the mixture yields a composite or an alloy capable of exhibiting desired properties. However, the choice of composite materials differ with applications. For example, carbon fiber reinforced composites are used for aircraft fuselage manufacturing where high specific strength characteristics is significant. The use of composites for the design of engineering structures is growing in the chemical, mechanical, aerospace, and oil and gas industries [4, 5, 6].

Equipment made from composite materials are used in the manufacturing industries for wide range of applications [1, 7, 8, 9, 10, 11, 12, 13, 14]. They can operate in various temperature ranges, where variations in temperature with time can give rise to the development of thermal stresses at microstructural levels, which can decrease the strength of the material [2]. Carbon fiber reinforced polymer (CFRP) is commonly used in engineering applications which require high strength-to-weight ratio and low thermal expansion [8]. An issue associated with this type of composite material is the non-uniformity in the microstructural element distribution, which may become a possible cause of thermal stress concentration leading to failure along the material interface. In addition, properties of the material could vary with a prolong exposure to unsteady temperature gradient [6].

There is limited knowledge on the thermo-elastic behaviour of this material at elevated temperatures. CFRP composite materials are obtained from thermosetting of polymer matrix, their thermal and mechanical properties deteriorate significantly when exposed to high temperatures (e.g. above 200 °C) [15, 16, 17]. Zhou et al. [13] showed that carbon fiber shrinks at elevated operating temperatures, causing the material tendons to deform longitudinally due to resin softening. Nikolaev et al. [18] studied the effect of constant and cyclic temperature

* Corresponding author.
E-mail address: echukwugozie@gmail.com (C.J. Ejeh).

https://doi.org/10.1016/j.heliyon.2020.e03622
Received 29 December 2019; Received in revised form 7 February 2020; Accepted 13 March 2020

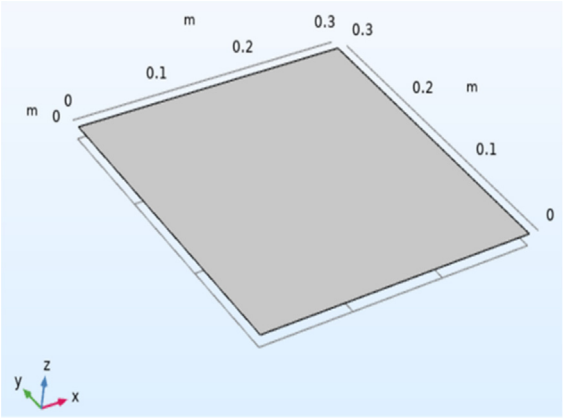

Figure 1. Cross sectional view of the laminate model geometry.

(−196 to 120 °C) on the mechanical properties of composite materials, where the sample were heated from interior using a spiral electric heater. They found that for higher thermal cycles, the strength, rigidity and rate of deformation increased significantly [18]. Similarly, Sayyad et al. [5] studied the thermo-elastic behavior of a laminated composite plate influenced by sinusoidal thermal load. Analytical approach based on the unified plate theory was used to determine the thermal stresses along plate interfaces and where assessed in view of the failure of the laminate. Masumi et al. [6] used first order shear deformation and layer-wise theory coupled with differential quadrature method (DQM) to study the thermal-mechanical property of a composite structure. Liu et al. [25] studied through numerical simulation the stress distribution created by compressing carbon fiber/epoxy braided composite materials. Hassanzadeh-Aghdam et al. [8] furthered this study by considering both thermal elastic-plastic behaviour of a nanocomposite reinforced with SiC nanoparticles using micromechanical cell method approach, however the effect of elevated heat intensity was not studied. The literature review on CFRP reveals that the structural integrity of this composite is strongly influenced by any temperature rise.

Hence, there is prevailing need for enhancement of this composite's thermo-elastic property, i.e. through re-structuring of the composite constituents or using resins reinforcement with nanoparticles. In the current work a composite shell composed of six (6) CRFP layers arranged in different stacking sequences is studied when subjected to deposited heat power in the range 10–200 W. This is equivalent to a temperature range 345–1200 K, which correspond to intense fire temperatures that could be experienced in applications of these composites. To quantify the ability of the composite to absorb and conduct the thermal load is the main objective of this study in addition to assessing the residual stresses in the composite due to thermal loading. A finite element model is developed for this purpose, which is validated with experimental results by Szpieg et al. [27] and Al-Qrimli et al. [28].

2. Methodology

2.1. Model description and discretization

The model geometry shown in Figure 1 represents a slice of the composite shell made from CFRP material. In total, the composite shell is composed of six (6) slices arranged in different stacking sequences as shown in Figure 2(a-d) with layer-wise arrangement of the composite shell layup, from bottom to the top. The stacked layers are positioned to be antisymmetric with reference to the mid-plane of the composite shell. The cross-sectional area of the model geometry is 30 × 30 cm with a thickness of 0.132 cm. The model geometry was created using the computer aided design tool in COMSOL Multiphysics software.

To analyse the impact of stacking sequences, the composite shell layers were arranged using the following stacking sequences (Case 1, 2, 3 and 4): [-70/45/-30/10/0/-80], [70/-45/30/-10/0/80], [45/-45/-60/60/60/-60] and [-45/45/45/-45/-45/45], which is motivated by Khedmati et al. [24] as composite layering arrangements for many applications in engineering. These arrangements were implemented through the layer-wise module in COMSOL software.

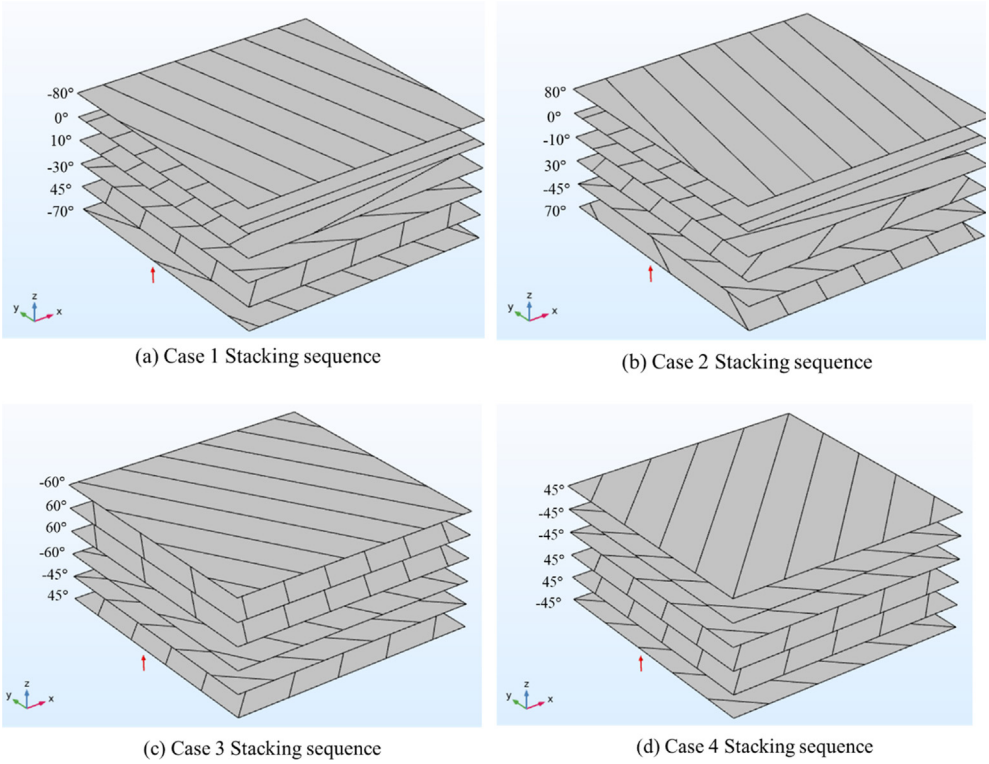

(a) Case 1 Stacking sequence

(b) Case 2 Stacking sequence

(c) Case 3 Stacking sequence

(d) Case 4 Stacking sequence

Figure 2. Model geometry showing layer stacking sequences for (a) case 1 (b) case 2 (c) case 3 and (d) case 4.

In COMSOL, the user controlled structured meshing option generates hexahedral elements that adapts to the physics settings of the model. Compared to unstructured and hybrid meshing style, structured meshing is numerically more accurate, ease of use code, and requires relatively lower computational time [29, 30]. Figures 3 and 4 show the discretized geometry and mesh sensitivity plot, respectively. Hexahedral elements were generated and evenly distributed through the domain. Mesh size is critical to ensure accuracy of the numerical solution and to ensure solution convergence, an element size convergence study is performed. In Figure 4 the change in Mises thermal stress with a beam power of 10 W versus number of elements used in the model is shown. The mesh sensitivity study shows that the solution converges after 2,021 elements.

2.2. Material properties

Commonly, Rule of Matrix (ROM) is often used to assign material properties. The coefficient of thermal expansion for both matrix and fiber properties were attained using ROM method [19]. It presents an easier approach to predict the material properties based on matrix and fiber volume fractions. Eqs. (1), (2), (3), and (4) are used for calculating the material density, modulus of elasticity along longitudinal and transverse direction, and strength, respectively, where ρ_c, ρ_f and ρ_m corresponds to composite, fiber and matrix density, respectively. In addition, V_f and V_m correspond the volume fraction of fiber and matrix, respectively [19].

$$\rho_c = \rho_f V_f + \rho_m V_m \tag{1}$$

Assuming a unidirectional reinforced composite material, the modulus of elasticity of the composite in the longitudinal direction (E_{cL}) can be estimated from Eq. (2) below [19].

$$E_{cL} = E_f V_f + E_m(1 - V_f) \tag{2}$$

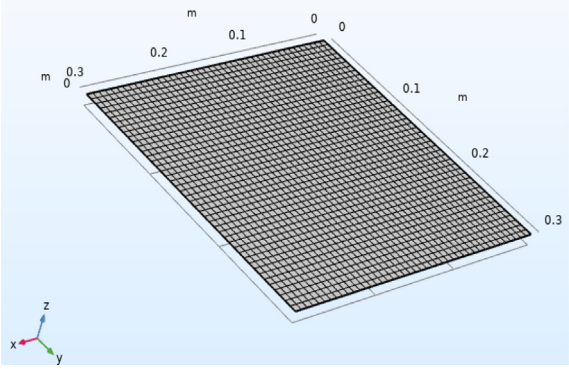

Figure 3. Model geometry meshing.

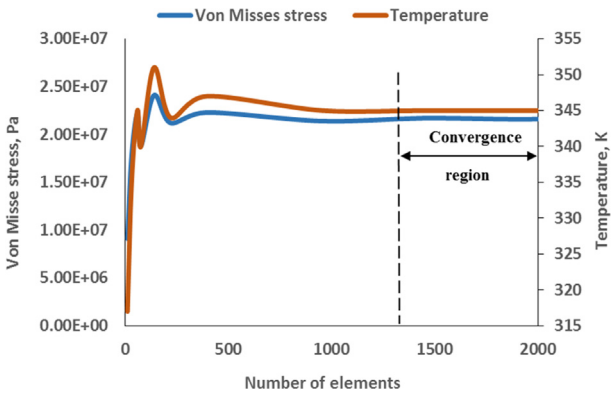

Figure 4. Mesh convergence study.

Table 1. Anisotropic material property.

Description	Value	Units
Fiber volume fraction	0.66	-
Matrix volume fraction	0.34	-
Fiber Young's modulus, fiber direction	230	GPa
Matrix Young's modulus	4.33	GPa
Fiber Poisson's ratio	0.24	-
Matrix Poisson's ratio	0.34	-
Fiber thermal expansion coefficient, fiber direction	-6.7×10^{-7}	1/K
Fiber thermal expansion coefficient, perpendicular to fiber direction	7.5×10^{-6}	1/K
Matrix thermal expansion coefficient	5.5×10^{-5}	1/K
Lamina thermal expansion coefficient, fiber direction	-1.389×10^{-7}	1/K
Lamina Poisson's ratio	0.274	-
Lamina thermal expansion coefficient, perpendicular to fiber direction	2.994×10^{-5}	1/K

Similarly, the elastic modulus along transverse direction (E_{cT}) is given by

$$\frac{1}{E_{cT}} = \frac{1}{E_m}V_f + \frac{1}{E_m}(1 - V_f) \tag{3}$$

From ROM, the strength and modulus of a continuous fiber reinforced composite are given in Eqs. (4), (5), (6), (7), (8), and (9) below.

$$\textit{for low } V_f, \qquad \varepsilon^*_m \le \varepsilon^*_f \;\; \sigma^*_c = \eta V_f \sigma'_f + (1 - V_f)\sigma^*_m \tag{4}$$

$$\textit{for high } V_f, \qquad \sigma^*_c = \eta V_f \sigma^*_f \tag{5}$$

$$\textit{for low } V_f, \qquad \varepsilon^*_m > \varepsilon^*_f \;\; \sigma^*_c = \eta(1 - V_f)\sigma^*_m \tag{6}$$

$$\textit{for high } V_f, \qquad \sigma^*_c = \eta V_f \sigma^*_f + (1 - V_f)\sigma'_m \tag{7}$$

$$\textit{For low } V_f, \qquad E^*_c = \eta V_f E^*_f + (1 - V_f)E^*_m \tag{8}$$

$$\textit{for high } V_f, \qquad E^*_c = \eta V_f \sigma^*_f \tag{9}$$

where η, σ, ε, V and E are the effectiveness parameter, tensile strength, ultimate strain at break, volume fraction and tensile stiffness, respectively. The superscripts * and $'$ refer to ultimate and maximum property values, respectively [19]. Also, η varies from 1 for unidirectional reinforcement to 5/8 in 2D random orientations [19].

Taking into consideration modelling aspect of the thermal properties for designing hybrid materials proposed by Ashby [20], the thermal properties for the composite laminate can be model in a similar way using the ROM equations. The thermal transverse conductivity of natural fiber composites is usually lower than in-plane conductivity [26]. The thermoplastic property of a typical carbon fiber composite can be obtained from Eqn. (10) and Eqn. (11) below. It should be noted that the

Table 2. Thermal properties of the composite material.

Description	Value	Units
Thermal conductivity of laminate, fiber direction	6.9	W/(m·K)
Thermal conductivity of laminate, perpendicular to fiber	0.54	W/(m·K)
Thickness of the laminate	1.32×10^{-4}	m
Cross sectional length	0.3	m
Initial deposited beam power	10	W
Heat transfer coefficient	30	W/(m^2·K)
Beam position along y-axis	0	m

transverse thermal conductivity of carbon fiber increases with a decrease in the volume fraction of the fiber (V_f), however this is not the case for in-plane, where the in-plane thermal conductivity increases with increasing V_f, which agrees well with the thermal conductivity of Fiber Reinforced Plastics (FRPs) [26]. The simplest approach used in the determination of material thermal conductivity in composites is ROM, and it is widely applicable for in-plane and transverse thermal conductivity determination. The in-plane conductivity can be determined using the parallel ROM in Eq. (10), where k_f, k_m and k_c correspond to the fiber and matrix conductivity, and the in-plane thermal conductivity of the composite, respectively [26]. The transverse thermal conductivity is determined using Eq. (11).

$$k_c = V_f k_f + (1 - V_f) k_m \tag{10}$$

$$\frac{1}{k_c} = \frac{1}{k_f} V_f + \frac{1}{k_m}(1 - V_f) \tag{11}$$

The model geometry was assigned anisotropic material properties as per the details in Tables 1 and 2 below. In addition, variations in material thermal conductivity was also considered. Furthermore, the tables provides good information on the non-linear elastic and thermal properties of the laminate.

2.3. Boundary settings

In setting up the boundary conditions, heat transfer in shells and thermal expansion of layered shell Multiphysics option is used. This was done to enable thermal interaction between the layered material and heat source, and to model heat transfer between objects in thermal contact. The heat beam module in COMSOL was used simultaneously with the heat transfer physics and the reference temperature at boundaries is set to ambient conditions.

Thermal insulation boundary condition was assigned to the four edges of the model geometry to minimise heat loss and to allow heat to be contained within the domain. Heat was applied at the center of the laminate and is transmitted from the top layer (layer 6) towards the bottom (layer 1). In addition, the beam orientation was positioned using the transformation vector $e = (0,\ 0,\ -1)$, which identifies the centre of the laminate. Convective heat flux and heat flow rate through layered material was modelled using Eqs. (12) and (13), where h is the heat transfer coefficient (W/m^{2}K), q is the heat flow rate, T_{ext} represent the external temperature (K), P_o is the beam power (W) and A is the cross sectional area (m^2).

$$q = h^*(T_{ext} - T) \tag{12}$$

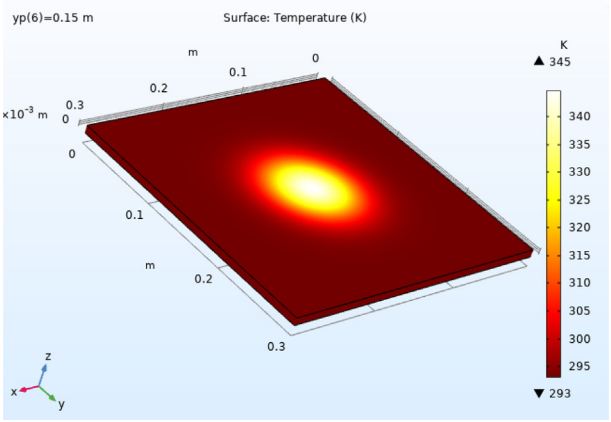

Figure 5. Surface temperature distribution with 10 W beam power.

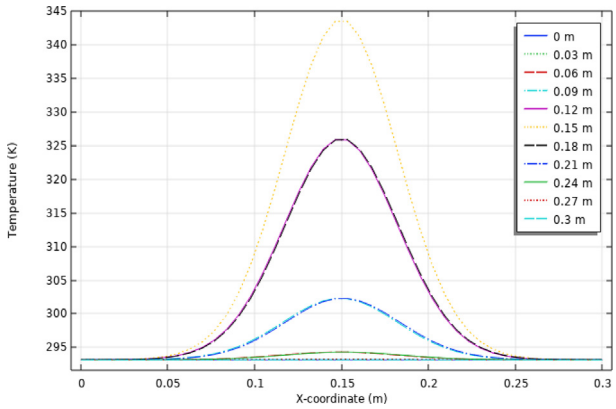

Figure 6. Tempereture distribution for different beam locations along (a) x-coordinate.

$$q_o = \frac{P_o}{A} \tag{13}$$

The boundaries with locus $x = 0$ and 30 cm is non-movable with conditions set at room temperature and pressure. A convective heat transfer coefficient of 30 W/m^{2}K was applied at first layer stack of the composite shell. The x and z-position of the beam source is fixed in space whilst varying its vertical position between 0 to 30 cm. The beam source standard deviation from its initial position is 1/10 of its height in the z-position which is equivalent to 0.3 cm.

3. Results and discussion

Numerical simulations using a non-linear solver were conducted and results are presented in this section. The bi-axial heat flux and temperature profile with position across the composite shell were investigated. The principal stresses and strains are obtained for heat power at 10W. The heat intensity is also increased to 200W to investigate the thermo-elastic response of the composite at elevated temperatures. In addition, the composite is doped with ceramic and glass nanoparticles and the residual stresses and deformations are obtained.

3.1. Variation of temperature with beam position

The beam was focused at the center point as shown in Figure 5, and the temperature contour is found to decay with distance from the center. The maximum recorded temperature have magnitude 345 K which is equivalent to 10 W beam power. Figures 6 and 7 describe the temperature profile in the x-direction and y-direction, respectively, showing that temperature is distributed non-linearly with space. This suggests that the

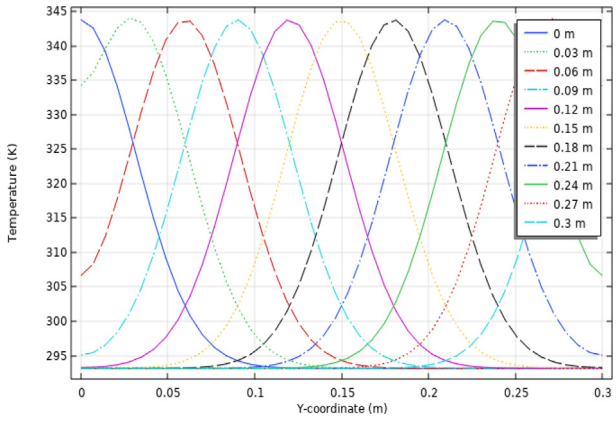

Figure 7. Tempereture distribution for different beam locations along y-coordinate.

induced thermal stress on the material will be unevenly distributed, leading to non-linear deformation of the composite shell. Analytically thermal stress distribution across a material can be predicted using empirical correlation that relates temperature and stress, but a compromise in accuracy of solution prediction is unavoidable.

3.2. Thermo-elastic deformation at low beam power

Generally, a material has a satisfactory thermo-elastic behaviour if it regains its original shape after being thermally loaded. Here, the thermo-elastic behaviour of the composite shell is determined through the obtained principal stresses and strains. In Figure 8, the stress and strain distribution along the *x-y, z-y* and *z-x* planes represent first, second and third principal axis respectively. The results were achieved for case 1 stacking sequence.

In general, the obtained principal stresses and strains is high for elevated temperatures [21,22,31]. The stresses and strains are found to be intense along the *x-y* plane, and minimal along at *z-x* plane, and thus elastic deformation is higher along this plane. Furthermore, it was observe that the composite deformed elastically under prevailing boundary conditions. The elastic behaviour of the composite depicts that the material offers good resistance to plasticity. The deformation axis is coplanar with the deposited heat power line of action, and spreads out un-evenly. The nonlinearity in the thermal stress and deformation pattern could be an outcome of the material orthotropic, and possibly layer orientations.

3.3. Model validation

The stress-strain relationship obtained from the numerical results were compared with those obtained by AL-Qrimli et al. [28] and Szpieg et al. [27]. AL-Qrimli et al. [28] studied the thermal-mechanical behaviour of carbon reinforced composite in typical fire conditions, while Szpieg et al. [27] performed similar study with carbon fiber reinforced maleic anhydride grafted polypropylene (MAPP) composite material. The comparative plots are provided in Figure 9 below. The plots demonstrate good correlation with about 5% error when compared to the results obtained by Szpieg et al. [27]. Therefore, the modelling approach

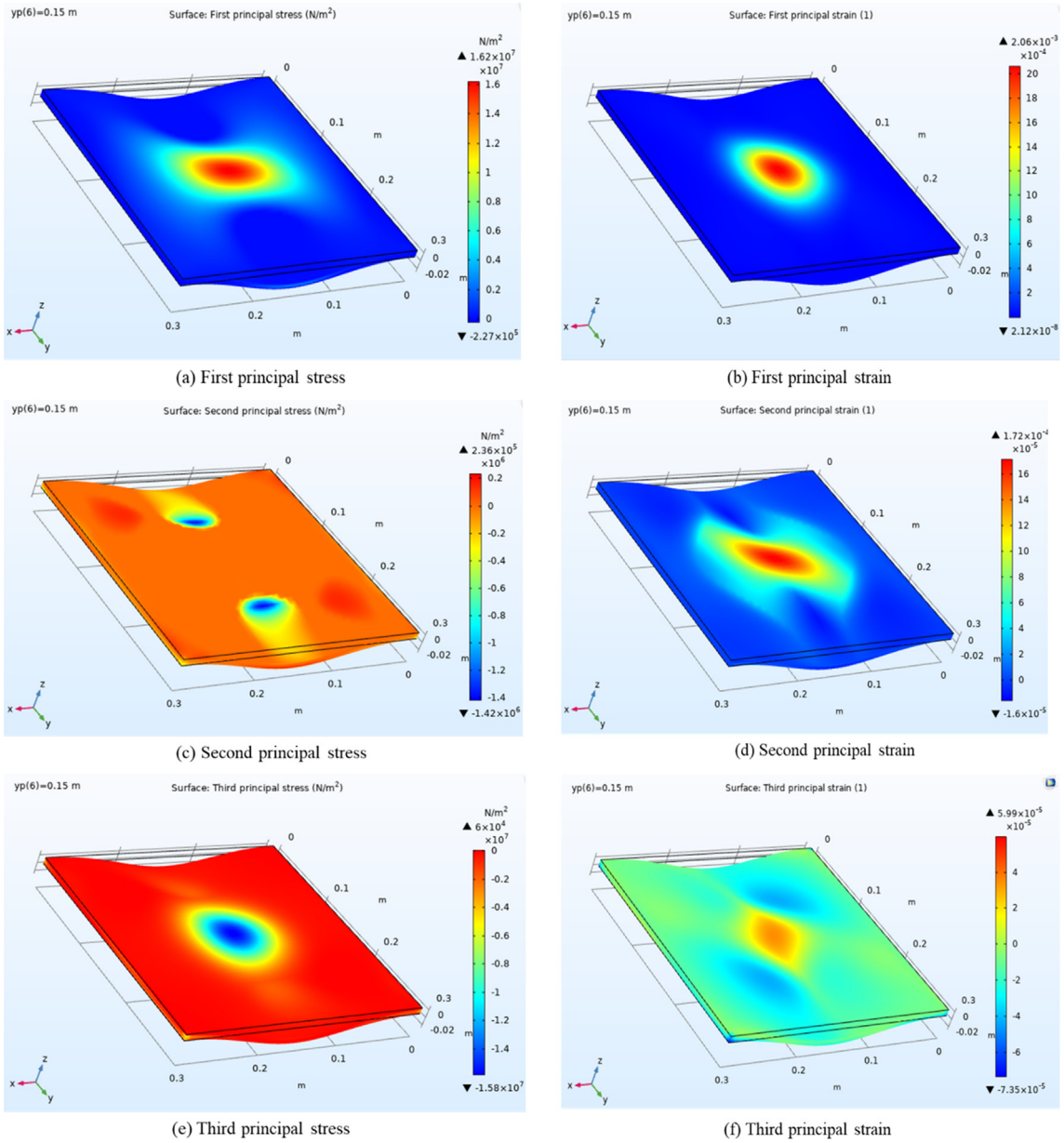

Figure 8. von Mises stress and strain contours pot for first, second and third principal axis.

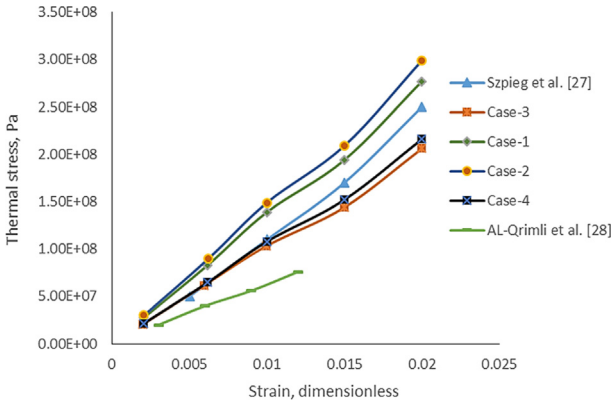

Figure 9. Thermal stress-strain relationship for variable deposited heat power.

utilized here gives reliable predictions of heat flux, temperature distribution, and thermal stress and strain distribution.

3.4. Effect of elevated beam power

A sensitivity study was conducted to investigate the effect of beam power and heat flux distribution to the stress and strain developed in the composite. The results are shown in Figures 10, 11, and 12. Heat flux, being a function of temperature gradient, provides good insight as to where the temperature gradient is maximum. Potential heat hotspots can be identified through this process. The plot relating heat flux, temperature and the variable beam power is presented in Figure 10. It is obvious that the magnitude of heat flux and temperature distribution in the laminate increases with beam power. The maximum heat flux and temperature predicted after 100 W beam power was 8.0×10^4 W/ m^2 and 900 K, respectively, and it is concentrated at the centre of the laminate where the beam is focused.

From Figure 11(a), it can be observ that the composite material show satisfactory thermo-elastic behaviour, as the material yield point is not reached regardless of an increase in deposited heat intensity. This was observed for all four cases considered. In addition, case 3 and case 4 show a better distribution of the induced thermal stresses compared to case 1 and case 2 due to the layer orientation and choice stacking sequence. Hence, layer orientation and stacking sequence has a significant effect on the thermal-mechanical response of composite materials in general. The strain shown in Figure 11(b) is observed to settle irrespective of an increase in temperature. The observation was pronounced for case 4 design. Therefore, case 4 design is preferred and will yield good thermo-elastic characteristics in engineering applications,. This is further confirmed by Liu et al. [23] work which involve optimization of blended composites wing panels using smeared stiffness technique. They proposed a stacking sequence with 0° and 90° difference in layer arrangement improves residual thermal stress management and distribution.

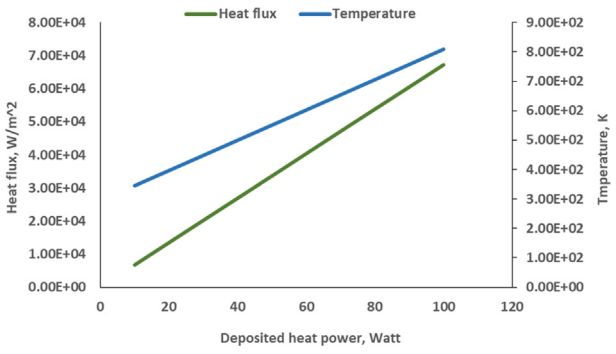

Fig. 10. Heat flux and temperature versus deposited beam power on the composite shell.

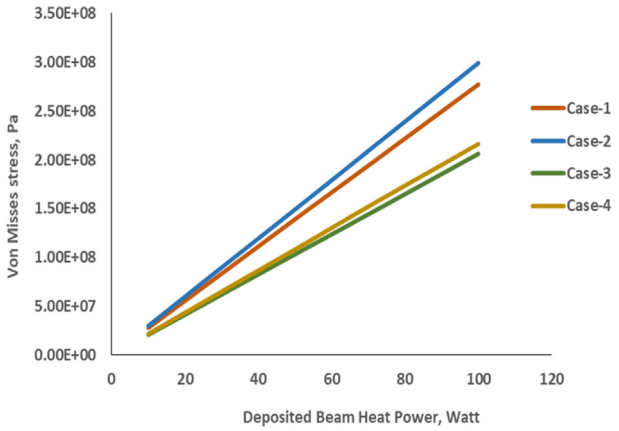

Figure 11. Mises stress versus deposited beam power on the composite.

This is in line with the findings for case 4, which has the ability to absorb and distribute the thermal load across its surfaces, thereby exhibiting good thermo-elastic characteristics.

3.5. Thermal stress distribution at layer slice

Qualitative analysis was also conducted to assess the stress and strain distribution, for all cases considered. As shown in Figure 14 Mises thermal stress distribution at the mid-plane of each layer of the laminate is shown. It shows that the load is distinctively affected by the layer arrangement. From Figure 14(d), the stress profile is fairly identical compared to its counterpart. It demonstrates that the case-4 material layer-wise arrangement is able to distribute the thermal load across its layers in the composite laminate. Hence, using case-4 stacking sequence for composite structures is suitable for thermal stress management.

Figures 14, 15, and 16 show the distribution of Mises stresses and the various components of the stress tensor with respect to the composite laminate coordinate system. The stress contours are derived from mid-plane of each composite layer, showing the effect of antisymmetric layer layup in the composite for a deposited beam heat power of 10W. This implies that the stress patterns in layer 1 and layer 6 of the composite laminate have very similar stress distribution, but are antisymmetric about the mid-plane of the laminate. The stress pattern for the stacking sequence case 4 (e.g. [-45/45/45/-45/-45/45]) was found to be suitable along the mid-plane, in-plane shear, and also through the transverse direction in the fiber direction of the laminate. Comparing Figure 13 with Figures 14, 15, and 16, thermal stresses are many experienced along the fiber direction of each laminate as compared to in-plane shear, mid-plane and transverse to the fiber direction of the laminate.

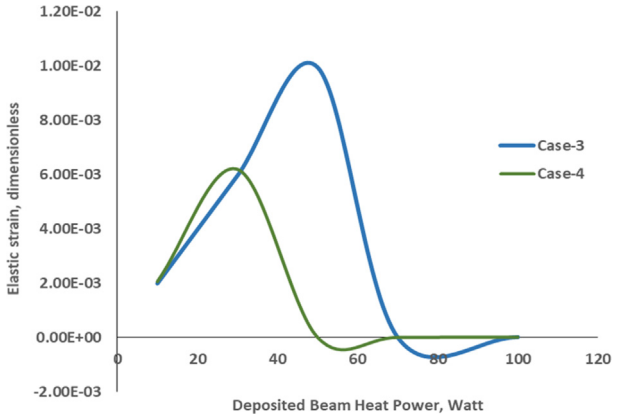

Figure 12. Strain versus deposited beam power on the composite.

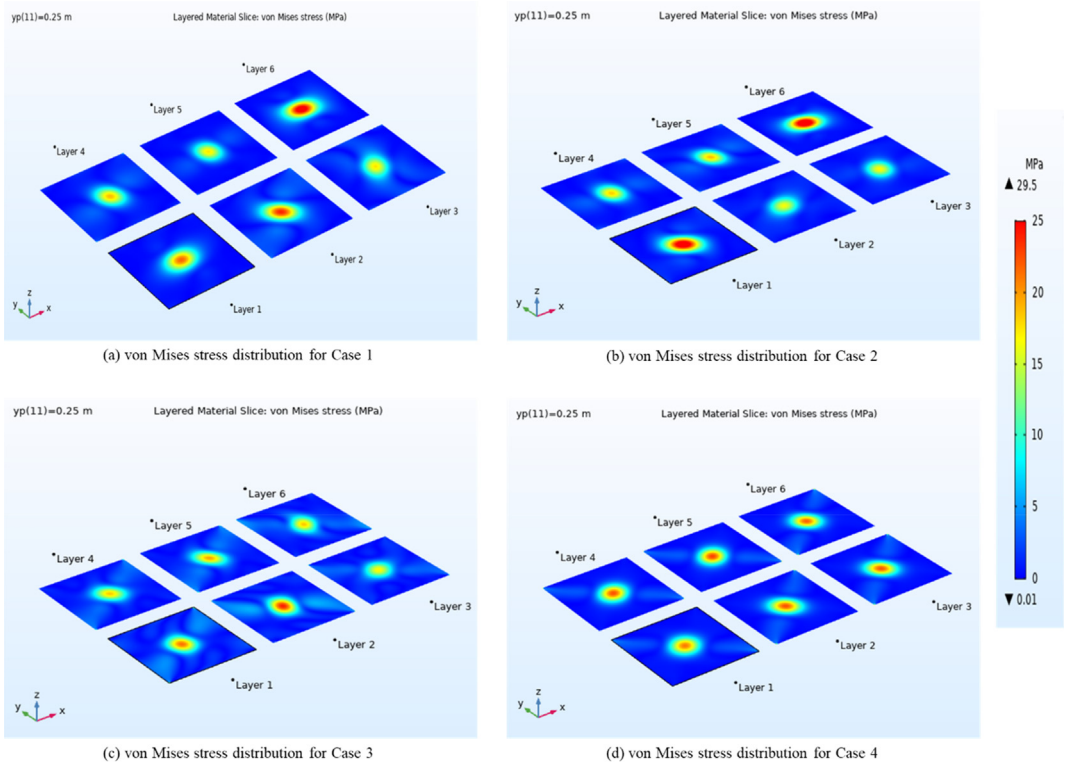

(a) von Mises stress distribution for Case 1

(b) von Mises stress distribution for Case 2

(c) von Mises stress distribution for Case 3

(d) von Mises stress distribution for Case 4

Figure 13. Mises thermal stress distribution at the mid-plane of each layer of the laminate with (at $y = 25$ cm): (a) case 1, (b) case 2, (c) case 3 and (d) case 4.

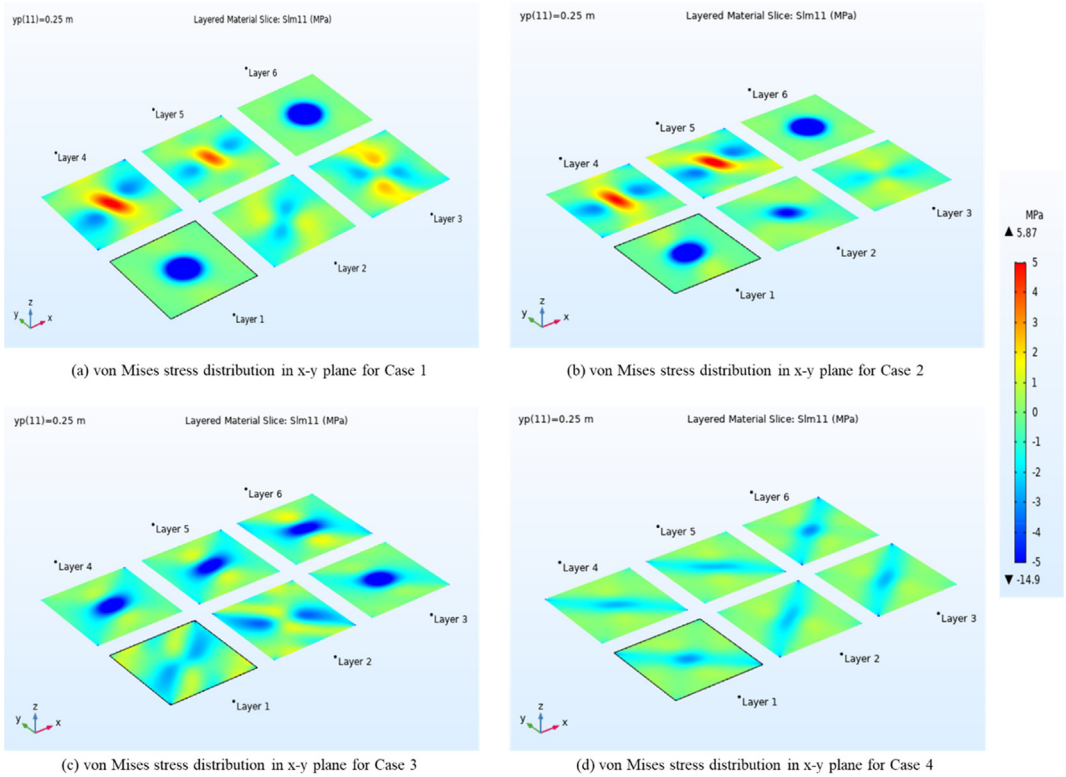

(a) von Mises stress distribution in x-y plane for Case 1

(b) von Mises stress distribution in x-y plane for Case 2

(c) von Mises stress distribution in x-y plane for Case 3

(d) von Mises stress distribution in x-y plane for Case 4

Figure 14. Thermal stress component along the fiber direction (x-direction) of each layer of the laminate (at $y = 25$ cm): (a) case 1, (b) case 2, (c) case 3 and (d) case 4.

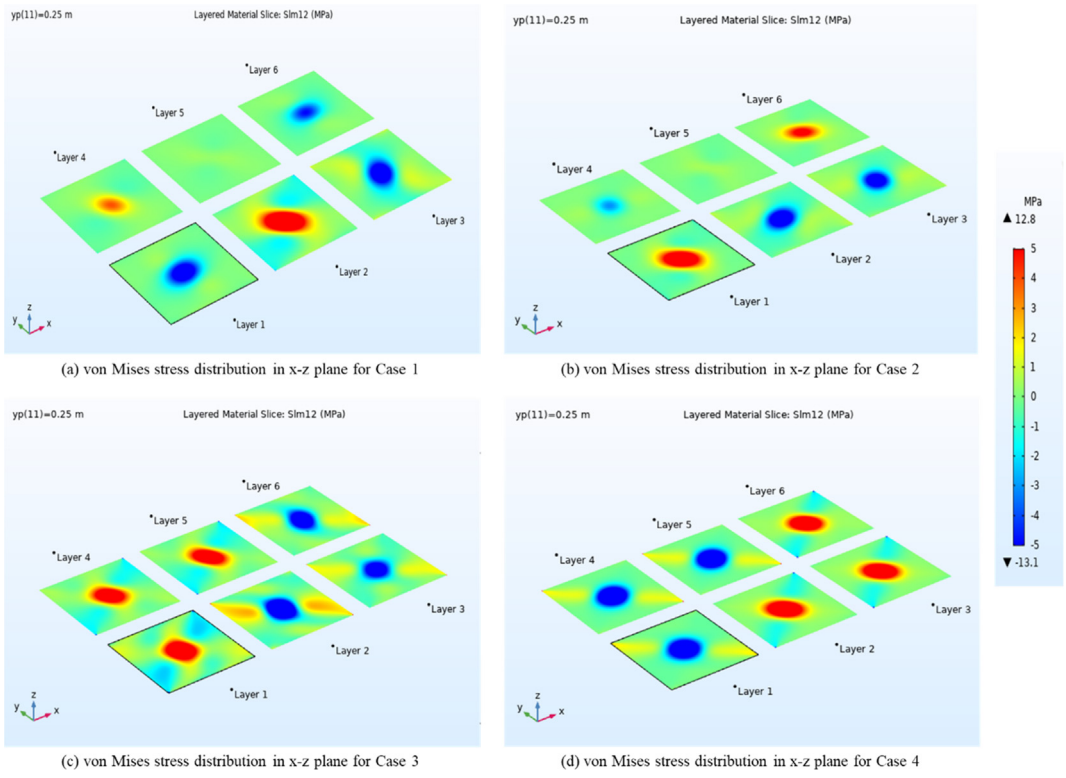

(a) von Mises stress distribution in x-z plane for Case 1

(b) von Mises stress distribution in x-z plane for Case 2

(c) von Mises stress distribution in x-z plane for Case 3

(d) von Mises stress distribution in x-z plane for Case 4

Figure 15. Thermal stress along the in-plane shear at the mid-plane of each layer of the laminate (at $y = 25$ cm): (a) case 1, (b) case 2, (c) case 3 and (d) case 4.

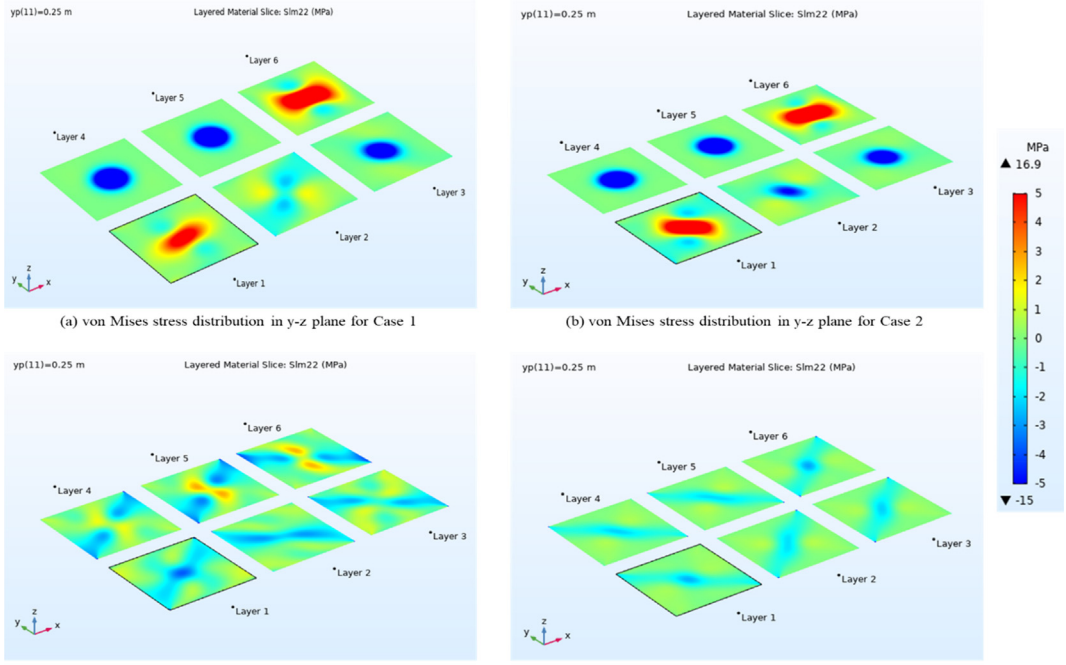

(a) von Mises stress distribution in y-z plane for Case 1

(b) von Mises stress distribution in y-z plane for Case 2

(c) von Mises stress distribution in y-z plane for Case 3

(d) von Mises stress distribution in y-z plane for Case 4

Figure 16. Thermal stress components transeverse to fiber direction at the mid-plane of each layer of the laminate (at $y = 25$ cm): (a) case 1, (b) case 2, (c) case 3 and (d) case 4.

3.6. Effect of doping with other materials

The previous section demonstrates that the composite shell is found to deform elastically under the influence of thermal loading. To evaluate the impact of doping, carbon fiber doped with silicon carbide (CFSiC) and using an alternative composite material such as resin-bonded glass fiber (RBGF) board were considered. Here, the deposited beam heat power was increased to 200 W for analytical purposes. The results obtained are shown in Figure 17 below. The results in Figure.17(b) and (c) depict that both the new cases, with CFSiC and RBGF, showed to be more thermo-elastic stable compared to the CFRP reference case 4 in Figure 17(a). In contrast, using SiC doped carbon fiber (CFSiC) is

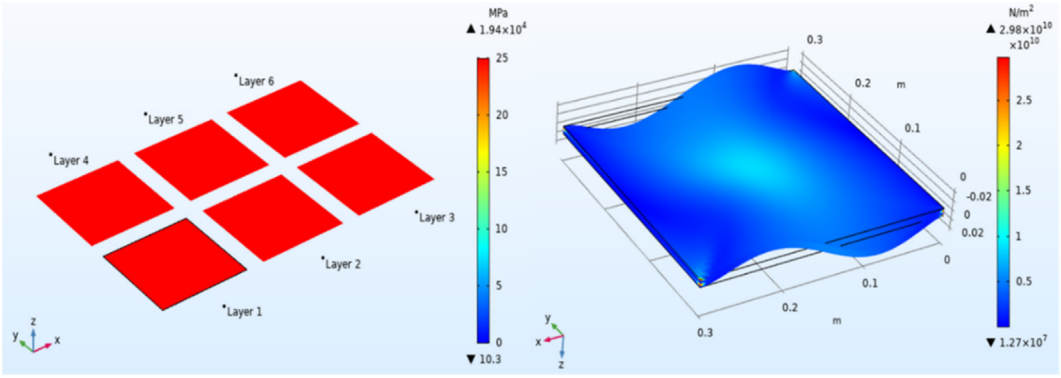

(a) Von Mises stress (left) and strain (right) for CFRP

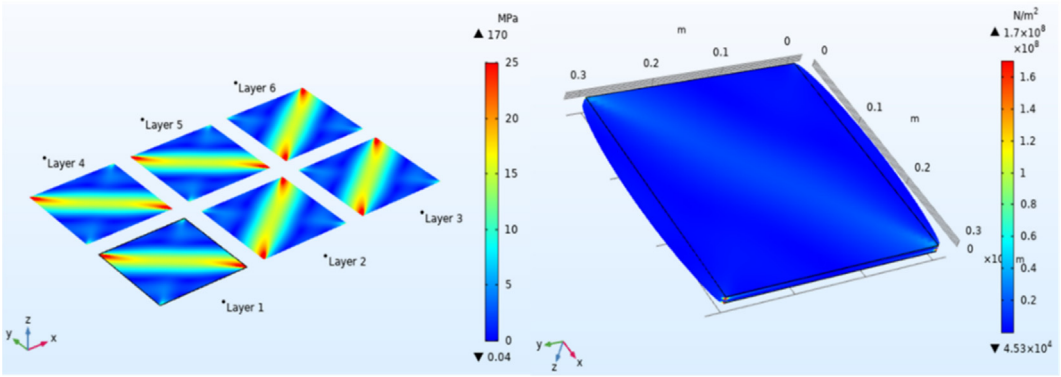

(b) Von Mises stress (left) and strain (right) for CFSiC

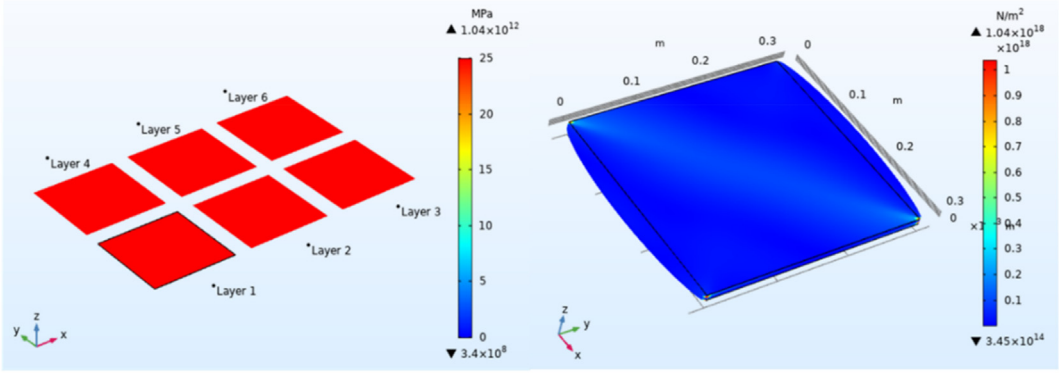

(c) Von Mises stress (left) and strain (right) for RBGF

Figure 17. Mises thermal stress along layered material slice: (a) CFRP, (b) CFSiC and (c) RBGF.

preferred compared to resin bonded glass fiber (RBGF) board for materials exposed to constant heat source. This is primarily due to one reason where the maximum stress distributed in the resin bonded glass fiber composite layered slice is pre-dominantly higher than those obtain from using SiC doped carbon fiber, despite its ability to resist deformation.

4. Conclusions

Findings based on the FEA study conducted suggest that CFRP composite material offers good resistance to thermal stress, even at elevated temperatures up to 800 K. The results were compared with Al-Qrimli et al. [28] and Szpieg et al. [27], and a good correlation was observed. However, it is recommended to conduct experiments to further validate the numerical results. The anisotropic material property assignment and stacking sequences had a significant effect on the thermos-elastic behavior. It shows that thermal stresses are relatively high along the carbon fiber direction and can be better managed when optimum stacking sequence is considered. Using carbon fiber doped with silicon carbide (CFSiC) obtained better thermo-elastic behaviour compared to CFRP and resin bonded glass fiber (RBGF) composite material.

Declarations

Author contribution statement

Chukwugoize Jekwu Ejeh: Conceived and designed the experiments; Performed the experiments; Analyzed and interpreted the data; Contributed reagents, materials, analysis tools or data; Wrote the paper.

Imad Barsoum: Analyzed and interpreted the data; Contributed reagents, materials, analysis tools or data; Wrote the paper.

Goodnews Ogbegbe Chizindu, Graham Martey Kodie & Josiah Ikechukwu Anachuna: Conceived and designed the experiments; Contributed reagents, materials, analysis tools or data.

Funding statement

This research did not receive any specific grant from funding agencies in the public, commercial, or not-for-profit sectors.

Competing interest statement

The authors declare no conflict of interest.

Additional information

No additional information is available for this paper.

Acknowledgements

Khalifa University is acknowledged for providing the platform which enabled successful completion of this work.

References

[1] D.N. Adnyana, Failure analysis of stainless steel heat exchanger tubes in a petrochemical plant, J. Fail. Anal. Prev. 18 (2) (2018) 413–422.
[2] C. Maharaj, A. Marquez, Failure analysis of a stainless steel pipe elbow in a purge gas line, J. Fail. Anal. Prev. 19 (1) (2019) 15–23.
[3] M.S. Kumar, M. Sujata, M.A. Venkataswamy, S.K. Bhaumik, Failure analysis of a stainless steel pipeline, Eng. Fail. Anal. 15 (5) (2008) 497–504.
[4] S. Gholizadeh, A review of non-destructive testing methods of composite materials, Procedia Struct. Integr. 1 (2016) 50–57.
[5] A.S. Sayyad, B.M. Shinde, Y.M. Ghugal, Thermoelastic bending analysis of laminated composite plates according to various shear deformation theories, Open Eng. 5 (1) (2015) 18–30.
[6] A.A. Masumi, G.H. Rahimi, G.H. Liaghat, Thermoelastic stress analysis in composite cylindrical vessel with metallic liner using first-order shear deformation theory and differential quadrature method, J. Thermoplast. Compos. Mater. 32 (2) (2019) 143–177.
[7] D. Tan, Q. Zhang, Application of carbon fiber in epoxy resin reinforcing in racing, in: Future Computer, Communication, Control and Automation, Springer, Berlin, Heidelberg, 2012, pp. 147–152.
[8] M.K. Hassanzadeh-Aghdam, M. Haghgoo, R. Ansari, Micromechanical study of elastic-plastic and thermoelastic behaviors of SiC nanoparticle-reinforced aluminum nanocomposites, Mech. Mater. 121 (2018) 1–9.
[9] R.M. Christensen, Mechanics of Composite Materials, Courier Corporation, 2012.
[10] S. Tsai, Introduction to Composite Materials, Routledge, 2018.
[11] L.A. Carlsson, D.F. Adams, R.B. Pipes, Experimental Characterization of Advanced Composite Materials, CRC press, 2014.
[12] T.W. Clyne, D. Hull, An Introduction to Composite Materials, Cambridge university press, 2019.
[13] A.G.E.D. Metcalfe, Interfaces in Metal Matrix Composites: Composite Materials, 1, Elsevier, 2016.
[14] E.J. Barbero, Introduction to Composite Materials Design, CRC press, 2017.
[15] R. Varleyl, K.H. Leong, Opportunities for nanocomposites in the oil & gas industry, in: Composite Technologies for 2020, Woodhead Publishing, 2004, pp. 557–562.
[16] V. Arumugaprabu, T.J. Ko, M. Uthayakumar, R.D.J. Johnson, Failure analysis in hybrid composites prepared using industrial wastes, in: Failure Analysis in Biocomposites, Fiber-Reinforced Composites and Hybrid Composites, Woodhead Publishing, 2019, pp. 229–244.
[17] F.R. Cichocki Jr., J.L. Thomason, Thermoelastic anisotropy of a natural fiber, Compos. Sci. Technol. 62 (5) (2002) 669–678.
[18] V.P. Nikolaev, E.V. Myshenkova, V.S. Pichugin, E.N. Sinitsyn, A.N. Khoroshev, Temperature effect on the mechanical properties of composite materials, Inorg. Mater. 50 (15) (2014) 1511–1513.
[19] D.K.Y. Tam, S. Ruan, P. Gao, T. Yu, High-performance ballistic protection using polymer nanocomposites, in: Advances in Military Textiles and Personal Equipment, Woodhead Publishing, 2012, pp. 213–237.
[20] M.F. Ashby, Materials selection in mechanical design, Metall. Ital. 86 (1994), 475-475.
[21] M. Fan, A. Naughton, J. Bregulla, Fire performance of natural fiber composites in construction, in: Advanced High Strength Natural Fiber Composites in Construction, Woodhead Publishing, 2017, pp. 375–404.
[22] A.A. Smerdov, O.A. Smerdova, L.P. Tanrova, et al., Experimental research of the stiffness and strength properties of carbon fiber-reinforced plastic, Konstr. Kompoz. Mater 3 (2009) 68–82.
[23] D. Liu, V. Toropov, M. Zhou, D. Barto, O. Querin, Optimization of blended composite wing panels using smeared stiffness technique and lamination parameters, in: 51st AIAA/ASME/ASCE/AHS/ASC Structures, Structural Dynamics, and Materials Conference 18th AIAA/ASME/AHS Adaptive Structures Conference 12th, 2010, p. 3079.
[24] M.R. Khedmati, M.R. Sangtabi, M. Fakoori, Stacking sequence optimisation of composite panels subjected to slamming impact loads using a genetic algorithm, Lat. Am. J. Solid. Struct. 10 (5) (2013) 1043–1060.
[25] S. Liu, B. Shi, A. Siddique, Y. Du, B. Sun, B. Gu, Numerical analyses on thermal stress distribution induced from impact compression in 3D carbon fiber/epoxy braided composite materials, J. Therm. Stresses 41 (7) (2018) 903–919.
[26] M. Fan, F. Fu (Eds.), Advanced High Strength Natural Fiber Composites in Construction, Woodhead Publishing, 2016.
[27] M. Szpieg, M. Wysocki, L.E. Asp, Mechanical performance and modelling of a fully recycled modified CF/PP composite, J. Compos. Mater. 46 (12) (2012) 1503–1517.
[28] H.F. AL-Qrimli, F.A. Mahdi, F.B. Ismail, Carbon/epoxy woven composite experimental and numerical simulation to predict tensile performance, Adv. Mater. Sci. 4 (2) (2015) 33–41.
[29] C.J. Ejeh, E.A. Boah, G.P. Akhabue, C.C. Onyekperem, J.J. Anachuna, I. Agyeibi, Computational fluid dynamics analysis for investigating the influence of pipe curvature to erosion rate prediction during crude oil transport, Exp. Comput. Multiph. Flow 2 (4) (2019) 255–272.
[30] C.J. Ejeh, G.P. Akhabue, I. Agyeibi, Effect of transient temperature on 304 stainless steel LPG tank structure using numerical simulation approach, SN Appl. Sci. 1 (2) (2019) 1690.
[31] F. Zhou, J. Zhang, S. Song, D. Yang, C. Wang, Effect of temperature on material properties of carbon fiber reinforced polymer (CFRP) tendons: experiments and model assessment, Materials 12 (7) (2019) 1025.